Supporting Information

Lanthanide dopant-induced formation of uniform sub-10 nm active-core/active-shell nanocrystals with near-infrared to near-infrared dual-modal luminescence

Daqin Chen[a], Yunlong Yu[a], Feng Huang[a], Hang Lin[a], Ping Huang[a], Anping Yang[a], Zhaoxing Wang[a,b], and Yuansheng Wang*[a]

[a] State Key Laboratory of Structural Chemistry, Fujian Institute of Research on the Structure of Matter, Chinese Academy of Sciences, Fuzhou, Fujian, 350002 (P. R. China)
[b] Fuzhou Overseas Chinese Middle School, Fuzhou, Fujian 350004

Figure S1-S11

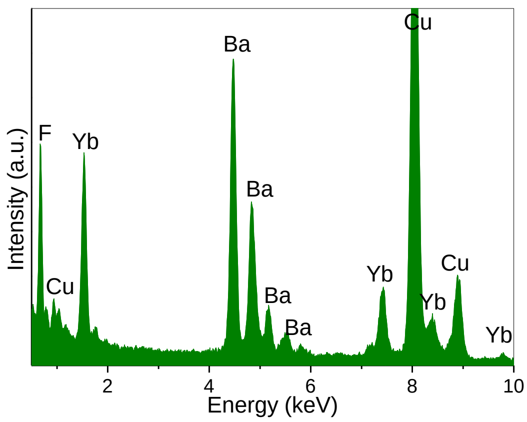

Figure S1. EDS spectrum taken from 0.3Tm^{3+},20Yb^{3+}:BaF_2 NCs, showing the existence of Ba, F and Yb elements (Cu signals come from the copper grid, Tm signal is not detected owing to the low doping content).

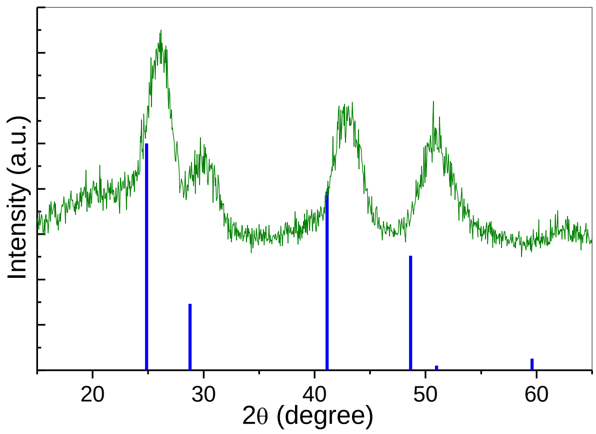

Figure S2. XRD pattern of 0.3Tm^{3+},20Yb^{3+}:BaF_2 NCs; the bars represent the standard cubic BaF_2 crystal data (JCPDS 04-0452).

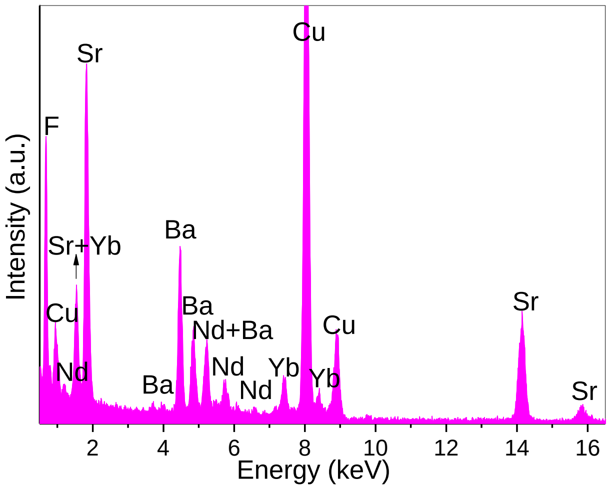

Figure S3. EDS spectrum taken from $0.3Tm^{3+},20Yb^{3+}:BaF_2/20Nd^{3+}:SrF_2$ active-core/active-shell NCs, showing the existence of Ba, Sr, F, Yb, and Nd elements (Cu signals come from the copper grid).

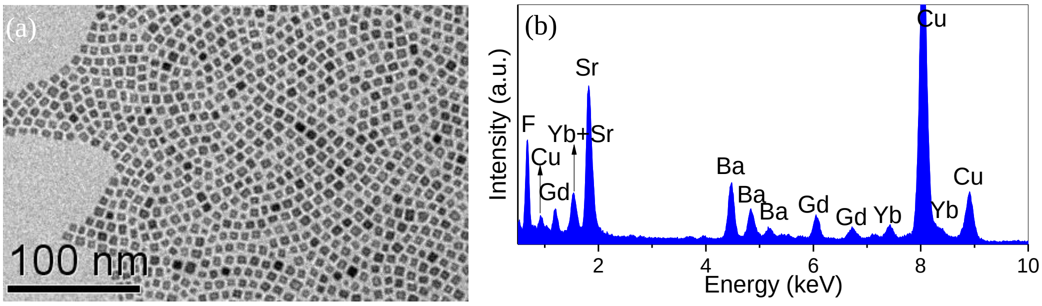

Figure S4. (a) TEM micrograph of $0.3Tm^{3+},20Yb^{3+}:BaF_2/20Gd^{3+}:SrF_2$ active-core/active-shell NCs; (b) EDS spectrum taken from NCs in (a), showing the existence of Ba, Sr, F, Yb, and Gd elements (Cu signals come from the copper grid).

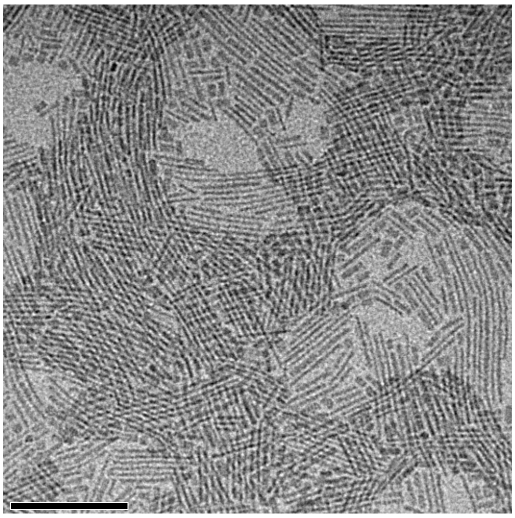

Figure S5. TEM micrograph of pure (un-doped) SrF_2 NCs prepared by thermolysis route using 80 mol% $Sr(CF_3COO)_2$ as reaction precursor.

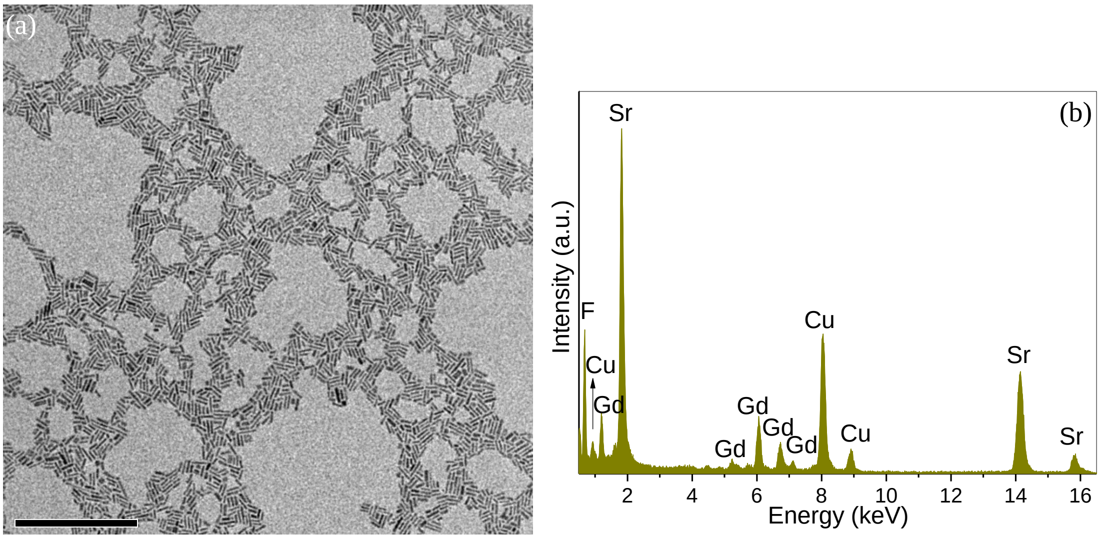

Figure S6. (a) TEM micrograph of $20Gd^{3+}$:SrF_2 NCs prepared by thermolysis route; (b) EDS spectrum taken from NCs in (a), showing the existence of Sr, F, and Gd elements (Cu signals come from the copper grid).

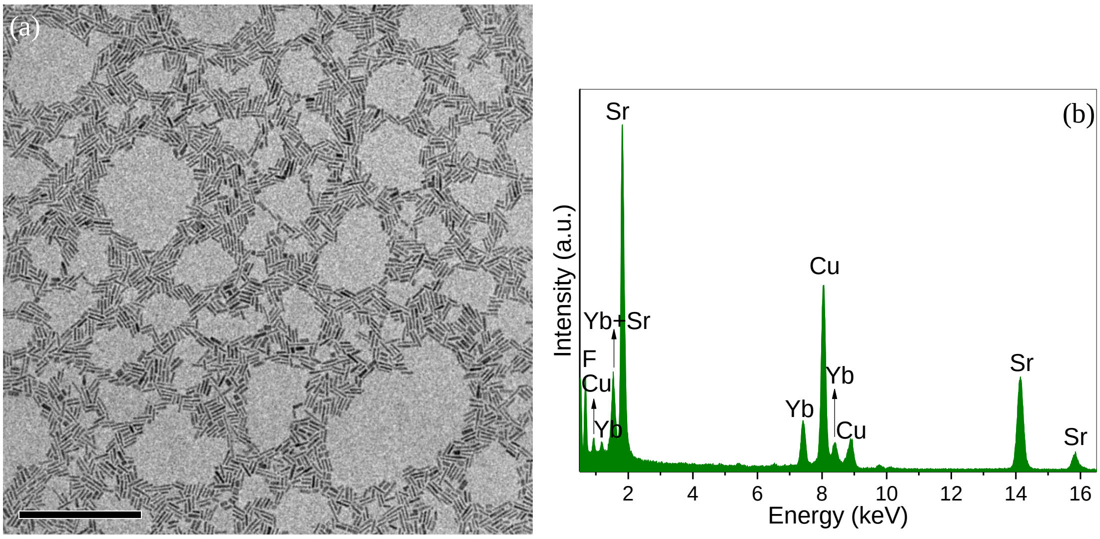

Figure S7. (a) TEM micrograph of $20Yb^{3+}$:SrF_2 NCs prepared by thermolysis route; (b) EDS spectrum taken from NCs in (a), showing the existence of Sr, F, and Yb elements (Cu signals come from the copper grid).

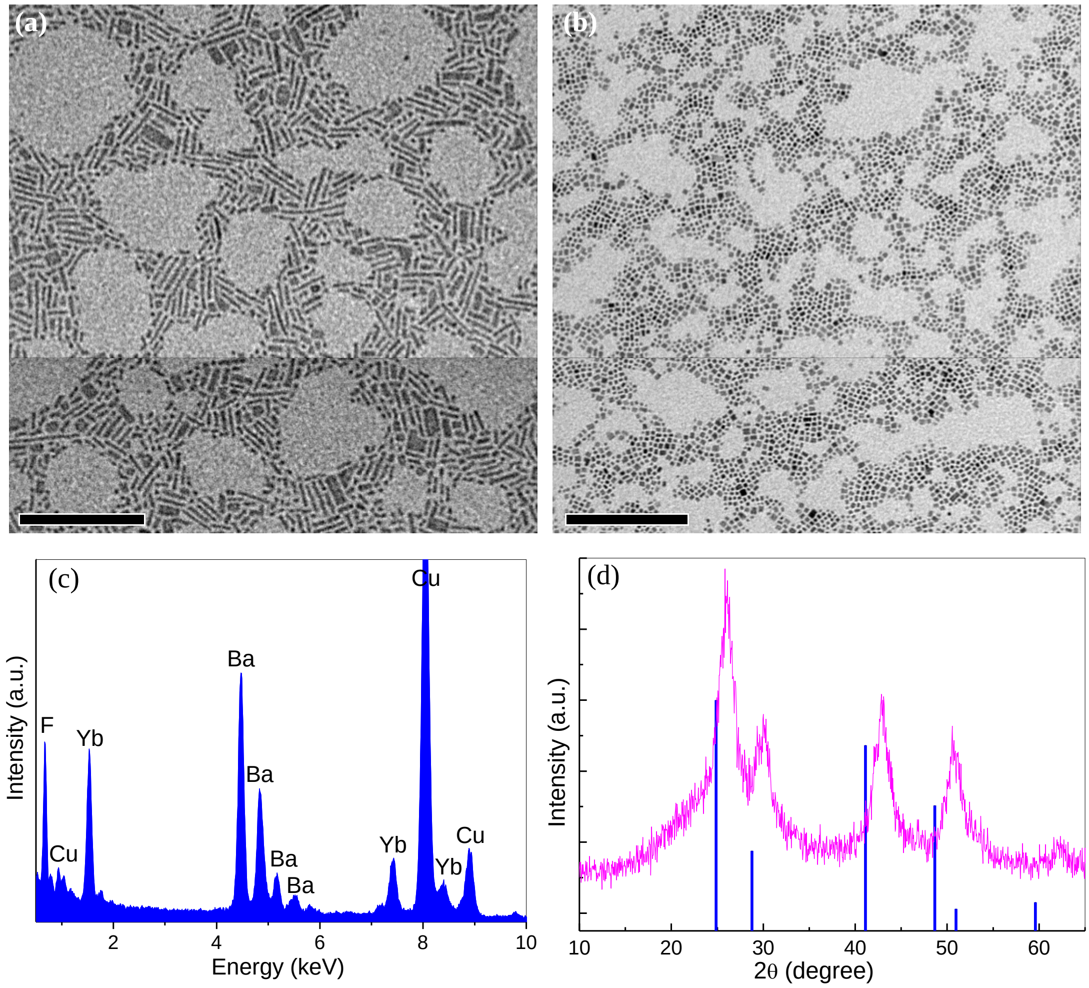

Figure S8. TEM micrographs of (a) pure BaF_2, and (b) $20Yb^{3+}$:BaF_2 NCs prepared by thermolysis route; (c) EDS spectrum taken from $20Yb^{3+}$:BaF_2 NCs, showing the existence of Ba, F, and Yb elements (Cu signals come from the copper grid); (d) XRD pattern of $20Yb^{3+}$:BaF_2 NCs, the bars represent the standard cubic BaF_2 crystal data (JCPDS 04-0452).

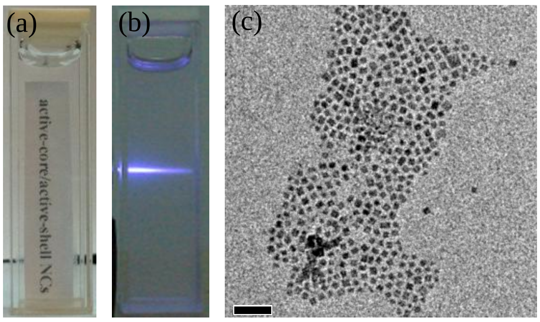

Figure S9. (a) TGA-modified $3Tm^{3+}$,$20Yb^{3+}$:BaF_2/$20Gd^{3+}$,$3Nd^{3+}$:SrF_2 active-core/active-shell NCs dispersed in water, (b) the corresponding UC luminescence photograph, and (c) TEM micrograph of TGA-modified $3Tm^{3+}$,$20Yb^{3+}$:BaF_2/$20Gd^{3+}$,$3Nd^{3+}$:SrF_2 NCs.

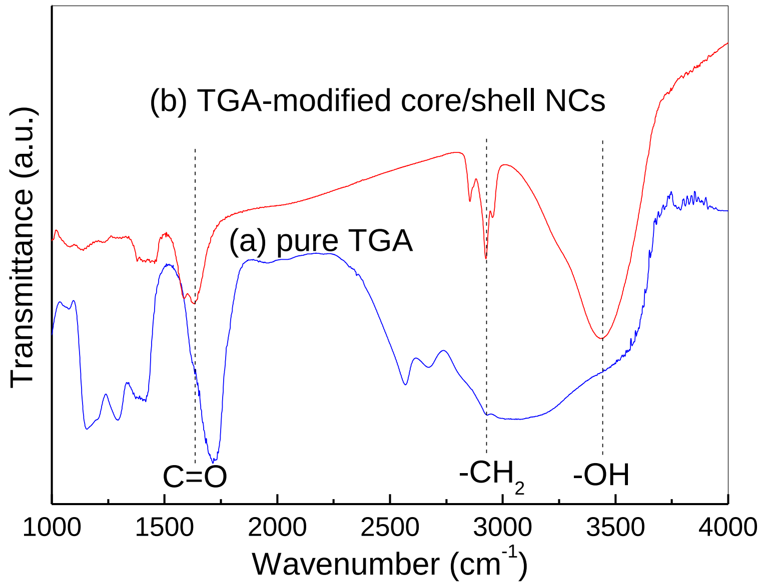

Figure S10. FTIR spectra of (a) pure TGA and (b) TGA-modified core/shell NCs.

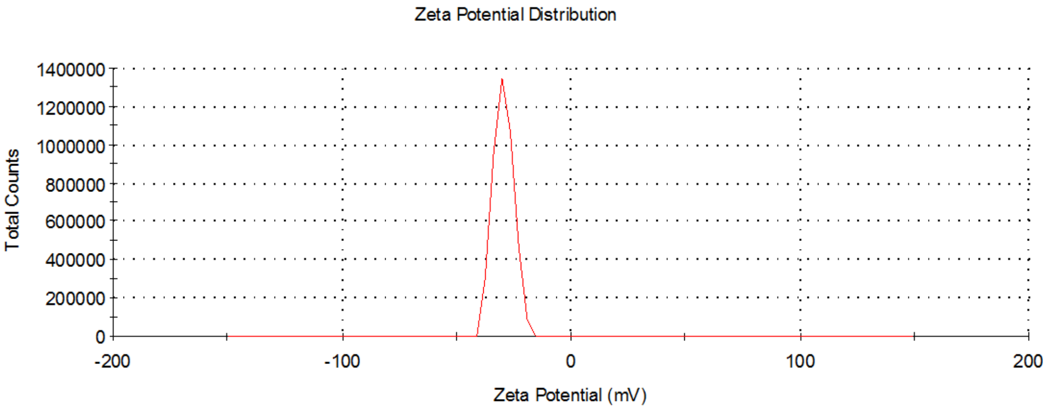

Figure S11. ζ-potential distribution of TGA-modified core/shell NCs dispersed in aqueous solution. The average ζ-potential is determined to be -30.5 mV.